

H²RSVLM: Towards Helpful and Honest Remote Sensing Large Vision Language Model

Chao Pang^{1*}, Jiang Wu^{2*},
Jiayu Li¹, Yi Liu¹, Jiaxing Sun⁵, Weijia Li³, Xingxing Weng¹, Shuai Wang⁴, Litong Feng⁴,
Gui-Song Xia^{1,5,6†}, and Conghui He^{2,4†}

¹School of Computer Science, Wuhan University ²Shanghai AI Lab ³School of Geospatial Engineering and Science, Sun Yat-Sen University ⁴Sensetime Research ⁵State Key Lab. of LIESMARS, Wuhan University
⁶Institute for Math & AI, Wuhan University

Abstract. The generic large Vision-Language Models (VLMs) is rapidly developing, but still perform poorly in Remote Sensing (RS) domain, which is due to the unique and specialized nature of RS imagery and the comparatively limited spatial perception of current VLMs. Existing Remote Sensing specific Vision Language Models (RSVLMs) still have considerable potential for improvement, primarily owing to the lack of large-scale, high-quality RS vision-language datasets. We constructed HqDC-1.4M, the large scale **H**igh **q**uality and **D**etailed **C**aptions for RS images, containing 1.4 million image-caption pairs, which not only enhance the RSVLM’s understanding of RS images but also significantly improve the model’s spatial perception abilities, such as localization and counting, thereby increasing the helpfulness of the RSVLM. Moreover, to address the inevitable “hallucination” problem in RSVLM, we developed RSSA, the first dataset aimed at enhancing the Self-Awareness capability of RSVLMs. By incorporating a variety of unanswerable questions into typical RS visual question-answering tasks, RSSA effectively improves the truthfulness and reduces the hallucinations of the model’s outputs, thereby enhancing the honesty of the RSVLM. Based on these datasets, we proposed the H²RSVLM, the **H**elpful and **H**onest **R**emote **S**ensing **V**ision **L**anguage **M**odel. H²RSVLM has achieved outstanding performance on multiple RS public datasets and is capable of recognizing and refusing to answer the unanswerable questions, effectively mitigating the incorrect generations. We will release the code, data and model weights at <https://github.com/opendatalab/H2RSVLM>.

Keywords: Remote sensing · VLM · Large-scale image caption dataset · Self-aware

1 Introduction

Recently, with the breakthroughs in Large Language Model (LLM) [2, 4, 48], large Vision-Language Models (VLMs) have rapidly evolved [3, 5, 28, 29, 36, 72]. These VLMs can deeply understand images and complete a variety of tasks, which has also driven the development of domain-specific VLMs [18, 24, 33]. The Remote Sensing (RS) imagery understanding is crucial for multiple fields such as the environment [61, 68], climate [20, 35], food security [22, 54], and disaster early warning [1]. The generic VLMs are perform poorly in the RS domain mainly due to two main reasons: First, remote sensing images, with unique characteristics, greatly differ from regular images, and understanding them requires specialized knowledge; second, the current generic VLMs typically use the CLIP [40] ViT [17] as visual encoder [3, 29, 50], but the spatial perception abilities of CLIP’s ViT are insufficient [37], affecting the VLMs’ spatial understanding capabilities [45].

Currently, the Remote Sensing specific Vision Language Models (RSVLMs) [19, 23, 34, 69] is typically trained from the pretrained weights of generic VLMs, therefore inheriting the aforementioned issues. Moreover, due to limited size of instruct-tuning data during the training process, the models are far from reaching an ideal state. Training with large-scale, high-quality RS vision-language datasets is the direct and effective means to solve the aforementioned problems. However, existing datasets have significant limitations, such as overly simple text descriptions that only focus on salient objects; or they contain a large number of non-RS images, leading to domain bias; or they are biased towards specific land features and lack diversity, as shown in Fig. 1 and Tab. 1. So, we created HqDC-1.4M dataset, the large scale **H**igh **q**uality and **D**etailed **C**aptions for RS images, containing 1.4 million image-caption pairs. The captions are generated by the powerful and

* Equal contribution. † Corresponding authors.



Fig. 1: Examples of large-scale RS vision-language datasets. RS5M [70] consists of two subsets: RS5M-RS3 and RS5M-PUB11. (a) HqDC-1.4M (ours) captions provide detailed descriptions, including **moving objects**, **rapidly changing information** (i.e. the seasonal feature in vegetation) and rich attributes of objects. (b) RS5M-RS3’s captions are short and lack detail. (c) RS5M-PUB11’s images are not typical RS images. The captions are short, repetitive texts, often containing **redundance** (such as “two houses” in the figure). (d) SkyScript [52] captions are from OpenStreetMap, therefore lacking moving objects and seasonal sensitive information; the descriptions are relatively short. (a) and (b) share the same image. We selected images of similar scene for (c) and (d).

advanced VLM Gemini-Vision [44]. The HqDC-1.4M dataset has three main features: Firstly, the captions are rich in information, covering the type, scene, and object details of the RS images, significantly enhancing the VLM’s understanding and recognition capabilities for RS imagery. Secondly, the captions are generated through carefully designed prompts, therefore include a wealth of attributes about local objects, such as quantity, color, shape, and spatial location. During training, these information can significantly improve the spatial detail capabilities such as location awareness and counting of the ViT [17] from CLIP [40] and the entire VLM. Thirdly, the dataset is large and comprehensive, covering RS images with resolutions from 0.1 to over 100 meters, and includes a rich variety of scene categories, ensuring the model’s wide applicability and excellent generalization capabilities. Therefore, the HqDC-1.4M greatly enhances the **helpfulness** of the RSVLM, which is validated through extensive experiments. Moreover, we have also constructed two instruct-tuning datasets, HqDC-Instruct and RS-Specialized-Instruct, enhancing the RSVLM’s multi-turn conversation and complex reasoning abilities, while also teaching the model with professional knowledge and skills in RS imagery processing.

Similar to the “hallucination” problem encountered with LLMs, VLMs inevitably face this issue during real-world applications [26, 27]. To reduce “hallucination” and become more **honest**, the key lies in teaching VLMs to be self-aware, i.e. recognizing the unanswerable question from users and refuse to answer it [51, 56]. This is particularly important when processing RS images, as the information that can be provided by the

Table 1: Comparison of HqDC-1.4M with other large scale RS vision language datasets. * means concurrent works. **Dynamic** means the texts contain moving objects and rapidly changing information over time such as seasonal sensitive information. **Avg. Len** means the average character length of captions in the dataset.

Datasets	#Images	Image Domain	Dynamic	Caption Type	Avg. Len
RS5M-PUB11 [70]	3M	Non-RS	Yes	list of phrases with redundancy	49
RS5M-RS3 [70]	2M	RS	Yes	list of phrases with redundancy	87
SkyScripts [52]	5M	RS	No	list of short phrases	56
LHRS-Align* [34]	1.15M	RS	No	long and fluent paragraph	unknown
ChatEarthNet* [62]	173k	RS	No	long and fluent paragraph	unknown
HqDC-1.4M	1.4M	RS	Yes	long and fluent paragraph	369


Text and Image Input Pair	Prior work	H ² RSVLM (ours)
 <p>Q1: What color is the top ship in the picture?</p>	<p>AI: The top ship in the picture is red.</p> <p>✓</p>	<p>AI: The top ship in the picture is red.</p> <p>✓</p>
<p>Q2: What is the actual color of the small vehicle in the remote sensing image?</p>	<p>A2: The actual color of the small vehicle in the remote sensing image is red.</p> <p>✗ (hallucination)</p>	<p>A2: The small vehicle in the picture is invisible, so I cannot provide an answer.</p> <p>✓ (honest)</p>

Fig. 2: When encountering unanswerable questions, the prior VLMs are probably to produce erroneous outputs, known as “hallucination”. Our H²RSVLM possesses strong honesty and can refuse to answer unanswerable questions.

images is inherently limited due to constraints in shooting angles and spatial resolution. Therefore, we created the first **Remote Sensing Self-Awareness** dataset, RSSA. Using RSSA, we train the RSVLM to possess the ability to refuse to answer unanswerable questions, as shown in Fig. 2, greatly enhancing the honesty of RSVLMs.

Based on the aforementioned data, we trained the **Helpful and Honest Remote Sensing Vision Language Model** (H²RSVLM). H²RSVLM achieves leading performance on multiple datasets for RS visual tasks compared with other generic VLMs and RSVLMs, demonstrating its helpfulness. Meanwhile, as shown in Fig. 2, H²RSVLM is able to recognize the unanswerable questions and refuse to answer, thus avoiding hallucinations, which shows its honesty.

The main contributions of this paper include:

- We constructed HqDC-1.4M, a large-scale dataset of 1.4 million remote sensing image and caption pairs. These high-quality, detailed captions could significantly enhance the remote sensing image understanding and spatial-detail perception of VLMs. Its large scale and diversity of images could ensure the VLM’s broad applicability and excellent generalization capabilities.
- We created RSSA, the first dataset in remote sensing field aimed at improving the model’s self-awareness, which contains a series of answerable and unanswerable tasks, effectively enhancing the honesty of RSVLMs and reducing the hallucinations.
- We proposed H²RSVLM, which possesses both helpfulness and honesty. It not only shows outstanding performance on remote sensing tasks, but also can recognize and refuse to answer the unanswerable questions thus avoiding hallucinations.

2 Related Work

2.1 Remote Sensing Vision Language Models

Inspired by the breakthroughs [2, 29, 34, 36, 40, 48] in LLMs and generic VLMs technology, many studies [19, 23, 65, 69] have begun to explore the application issues of VLMs in the field of RS. These efforts mostly

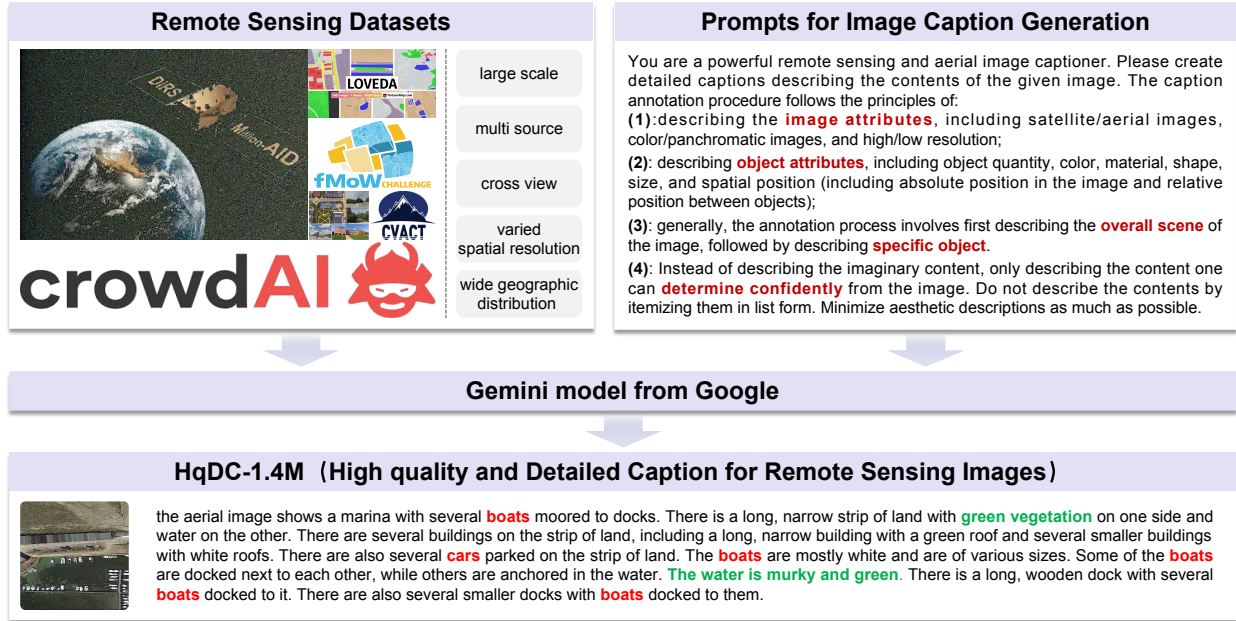


Fig. 3: The construction pipeline of HqDC-1.4M dataset. We utilize images from publicly available remote sensing datasets and design effective prompts to induce Google’s commercial Gemini-Vision model to generate captions for remote sensing images.

focus on how to construct high-quality instruction data to finetune generic VLMs, enabling them to handle common RS visual tasks. For example, GeoChat [23] adopted the approach from LLaVA [29] to build a fine-tuning instruction dataset, introducing region-based question-answering and grounding functions into RSVLM. EarthGPT [69] expanded input images to SAR images and infrared images. However, these studies only utilized large-scale natural image text data for pre-training, a training strategy that is not ideally suited for RSVLMs. Furthermore, these models were not designed with the consideration that they need to have self-awareness and be able to refuse to answer certain questions. Therefore, we leverage large-scale RS image-text pair data to enhance category perception ability and explore improving the honesty for RSVLMs.

2.2 Large-scale Remote Sensing Vision Language Datasets

In recent years, there have been some large-scale visual language datasets [34, 52, 62, 70] emerging in the field of RS. Some of these datasets primarily focus on training CLIP [40] models for RS applications, serving zero-shot scene classification, image retrieval, and other image-level tasks. Therefore, these datasets [52, 70] mainly provide brief descriptions of the scene type or the type of objects at the center of the image, with limited information. For example, The RS5M [70] dataset is divided into two parts. The first part includes remote sensing images and their corresponding annotations, which were selected from 11 public large-scale English natural image-text paired datasets. The second part consists of images chosen from three publicly available remote sensing databases: MillionAID [32], fMoW [11], and BigEarthNet [42]. For these images, brief captions were generated using the BLIP [25] model. SkyScript [52] matches Google images with the OpenStreetMap (OSM) database and selects relevant image attribute values from OSM to concatenate them as image captions. Our concurrent work LHRs-Align [34] used the similar method to extract several attribute values from OSM and then summarize them using Vicuna [10] to generate long and fluent captions. Another concurrent work [62] inputs labels from existing segmentation datasets into ChatGPT [2] to generate image descriptions based on segmentation categories. These caption datasets mostly overlook the category information provided by dynamic objects in the images, let alone include relative positioning information of multiple objects. In contrast, we propose using the powerful commercial VLM Gemini-Vision to generate high-quality fine-grained caption datasets, including category, attributes, and positional descriptions of both fixed and moving objects, as shown in Tab. 1.

Table 2: Image sources of HqDC-1.4M.

Image source	#images	GSD (m)
Million-AID [32]	920057	0.5-153
CrowdAI [12]	276344	<0.5
fMoW [11]	81224	-
CVUSA [53]	44416	0.08
CVACT [30]	44416	0.12
LoveDA [49]	23948	0.3
Total	1390405	-

2.3 Self-Aware Language Model and Vision Language Models

Some research has focused on the self-awareness capability of LLMs [8, 15, 60, 67] and VLMs [51, 56], that is, the ability to be aware of one’s own ignorance when faced with unknown or unanswerable questions and therefore choose not to answer. In LLM research, SelfAware [60] carefully constructed a dataset consisting of unanswerable or unknowable questions to evaluate the LLM’s ability to recognize the unknown knowledge. [8] went on to create a “I don’t know” training dataset to improve the LLM’s capacity to acknowledge its own lack of knowledge and decline to respond.

In the field of VLMs, MM-SAP [51] introduced the concept of a "knowledge quadrant" specific to VLMs, which categorizes concepts within perception tasks into known and unknown quadrants. Furthermore, they created an inaugural benchmark to assess the self-awareness proficiency of VLMs in these tasks. [56] proposed a cascading approach, first determining if there is an error in the question, then informing the user of the error in the question, and in appropriate scenarios, correcting the question and providing an answer. We also followed the path of general LLMs and VLMs, creating the RSSA dataset to investigate the self-awareness capabilities of RSVLMs.

3 Helpful and Honest Datasets for RSVLMs

To enhance the helpfulness of RSVLMs, we constructed three RS vision-language datasets: HqDC-1.4M, HqDC-Instruct, and RS-Specialized-Instruct. To improve the honesty of RSVLMs, we constructed the first Remote Sensing Self-Awareness dataset, RSSA. Next, we will introduce these datasets.

3.1 HqDC-1.4M Dataset

Inspired by ShareGPT4V [6], we utilized the “gemini-1.0-pro-vision” API ¹ to generate descriptions for images from multiple public RS datasets, thereby obtaining a dataset of image-text pairs to serve as the pre-training data for RSVLMs, as shown in Fig. 3. We have designed appropriate prompts to guide the Gemini-Vision model to provide detailed descriptions of remote sensing images, including the type and resolution of the images, as well as information on the attributes, quantities, colors, shapes, spatial positions of objects in the images. This ultimately results in organized, detailed, and comprehensive descriptions. This prompt is displayed in Fig. 3. The information of the source image we selected is shown in Tab. 2. The selected RS images have a Ground Sample Distance (GSD) ranging from 0.1 meters to over 100 meters. They contain a wide spatial distribution and a diverse range of landcover types [32], making them highly representative and practical for downstream RS tasks. In response to the oversized images in the original dataset, we cropped them into small images of 512×512 pixels. In the end, we generated approximately 1.4 million of high quality and detailed captions of RS images.

To evaluate the quality of the HqDC-1.4M dataset, we randomly sampled 140 image-text pairs for manual inspection based on the proportion of the original image dataset. We segmented each long caption by periods, resulting in a total of 851 sentences. Based on the comparison of images and descriptions, we categorized the sentences into the following three types:

¹ https://ai.google.dev/docs/gemini_api_overview

Table 3: Information of RSSA dataset. The training images of all tasks are from DOTA-v2-train [16] and FAIR1M-train [43]. MCQ stands for Multiple Choice Question.

Tasks	Question Type	Test-set Source	#Train Sample	#Test Sample
<i>Presence</i>	Yes-or-No	DOTA-v2-test	ans: 8000	ans: 242
<i>Color</i>	Open-ended	DOTA-v2-test FAIR1M-val	ans: 8000 unans-pan: 1000 unans-invis: 4000	ans: 200 unans-pan: 100 unans-invis: 300
<i>AbsPos</i>	MCQ	DOTA-v2-test	ans: 8000 unans: 4000	ans: 100 unans: 300
<i>RelPos</i>	MCQ	DOTA-v2-test	ans: 8000 unans: 4000	ans: 100 unans: 300

- Type I, descriptions are entirely accurate: The provided information can be directly obtained from the RS images and is completely accurate.
- Type II, descriptions are partially accurate: The information provided is partially incorrect but partially correct, thus still holding some value.
- Type III, descriptions are entirely incorrect: The information provided is entirely incorrect.

Examples of each type can be found in the Appendix A. Through manual annotation, the proportions of these three categories are 0.69, 0.20, and 0.11, respectively. It is evident that the vast majority of sentences in the HqDC-1.4M dataset are accurately described, effectively conveying the information provided by the RS images and offering valuable information for the training of RSVLMs.

The sample examples of HqDC-1.4M and several other large-scale RS image-text pair datasets can be found in Fig. 1, while detailed comparative information is available in Tab. 1. A key feature of our HqDC-1.4M dataset is the use of high-performance large multimodal language models, resulting in more detailed, coherent, information-rich, and non-redundant descriptions. This dataset covers static land types, and rapidly changing information over time, such as dynamic objects (e.g., vehicles, ships) and seasonal sensitive information (such as vegetation descriptions in temperate summer and winter). Therefore, the RSVLMs trained on HqDC-1.4M exhibit superior performance, as detailed in Sec. 5.4.

3.2 HqDC-Instruct Dataset


Following LLaVA [29], we created the dataset HqDC-Instruct for fine-tuning RS-VLM. This dataset comprises 30k RS images, with 26k dedicated to conversation and 4k to complex reasoning. We selected two RS object detection datasets, DOTA-v2 [57] and Fair1M [43], as the sources of our images. Subsequently, we utilized the method introduced in Sec. 3.1 to generate detailed captions for these images using the Gemini-Vision model. Next, similar to LLaVA [29], we combined the aforementioned descriptions with the original object detection annotations of the dataset and input them into the language-only Gemini. Through carefully designed prompts and few-shot examples, we guided the Gemini language model to generate multi-turn conversation and reasoning data. The detailed prompts and in-context examples are shown in Appendix B.

3.3 RSSA Dataset

To enhance the honesty of VLMs and enable them to accurately identify and reject the unanswerable questions, we have created the RSSA dataset. It contains four main tasks:


- Object Presence Question Answering (*Presence*): The purpose of this task is to confirm whether a specified type of object exists within the provided RS image. The question format is yes-no.
- Object Color Question Answering (*Color*): This task focuses on asking about the actual color of a specified object within an image. The question format is open-ended.
- Object Absolute Position Question Answering (*AbsPos*): This task is used to determine the precise location of a specified object within an image. The question format is multiple-choice.
- Object Relative Position Question Answering (*RelPos*): This task is used to understand the relative positional relationship between two objects within an image. The question format is also multiple-choice.

(a) Presence

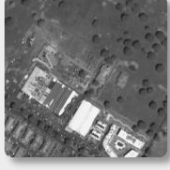


Answerable:
Q: Is there a large vehicle in the image?
 Just answer yes or no.
A: yes


(b) Color



Answerable:
Q: What is the actual color of the plane in the remote sensing image? If this question is unanswerable, please provide the reason.
A: white




Unanswerable (panchromatic):
Q: Please specify the actual color of the swimming pool in this aerial image. If this question is unanswerable, please provide the reason.
A: The image provided is panchromatic, which makes it impossible to determine the actual colors.




Unanswerable (invisible)
Q: What is the actual color of the tennis court in the remote sensing image? If this question is unanswerable, please provide the reason.
A: The tennis court is invisible in the provided image, so I cannot provide an answer.

(c) AbsPos




Answerable:
Q: Where is the baseball diamond located in the image?
A: Sorry, the object is invisible B: right C: center D: left E: bottom right
A: D




Unanswerable:
Q: Whereabouts in the aerial image is the soccer ball field?
A: center B: top right C: bottom right D: Sorry, the object is invisible E: top left
A: D

(d) RelPos



Answerable:
Q: Where is the large vehicle in relation to the small vehicle?
A: To the top right of the small vehicle B: To the inside of the small vehicle C: To the left of the small vehicle D: Sorry, at least one object is invisible E: To the bottom right of the small vehicle
A: C



Unanswerable:
Q: Where is the plane in relation to the small vehicle?
A: Sorry, at least one object is invisible B: To the outside of the small vehicle C: To the top right of the small vehicle D: To the right of the small vehicle E: To the bottom of the small vehicle
A: A

Fig. 4: Sample examples in RSSA dataset.

The three tasks, *Color*, *AbsPos* and *RelPos*, all involve inquiring about specific attributes of the object in the image, and include both answerable (**ans**) and unanswerable (**unans**) questions. In task *Color*, there are two types of unanswerable questions: one is that the object does not exist or is not visible in the image (**unans-invis**); the other is if the image is a panchromatic RS image, then it is impossible to determine the actual color of the object (**unans-pan**). As for task *AbsPos* and *RelPos*, the question is unanswerable if the objects mentioned do not exist or are not visible in the corresponding image.

We built our RSSA dataset based on two RS object detection datasets, DOTA-v2 [16] and Fair1M [43]. For the images in the original datasets that are too large, we have cropped them into smaller images of size 512×512.

4 H²RSVLM

We train the **helpful** and **honest** remote sensing vision language model (H²RSVLM) with the datasets introduced in Sec. 3.

4.1 Model Architecture

We adopted the LLaVA model [29] and continued to train it to obtain the H²RSMVL. It includes three main components:



Fig. 5: Training stages of H²RSVLM.

- The pretrained vision encoder using the CLIP-Large model [9] with a resolution of 336×336 and a patch size of 14, capable of converting input images into 576 tokens.
- The LLM based on the open-source Vicuna-v1.5 [10], originating from LLaMA2 [48]. We use the 7B-version throughout this paper.
- The projector, which is a multilayer perceptron (MLP) composed of two layers, used to connect the vision encoder and the LLM.

Our training is divided into two stages: the first stage is pretraining, and the second stage is supervised fine-tuning, as shown in Fig. 5.

4.2 Pretraining

We pretrain the H²RSVLM using HqDC-1.4M dataset. We load the pretrain weights of LLaVA [29] model as initialization. During the pretraining process, unlike previous models, we fine-tune the vision encoder, LLM, and projection layer simultaneously. We trained for a total of 1 epoch, with a batch size set to 256, and approximately 5400 steps of iteration. The same learning rate strategy is applied to all modules: a cosine schedule, with a base learning rate of $2e-5$. All the pretraining experiments were conducted on 16 NVIDIA A100-80G GPUs.

4.3 Supervised Fine Tuning

The training datasets during the Supervised Fine Tuning (SFT) stage comprise four parts, each with a specified quantity: the HqDC-Instruct dataset (30k), the RSSA dataset (44k), the RS-Specialized-Instruct dataset (29.8k), and the RS-ClsQaGrd-Instruct dataset (78k), summing up to a total of 180k.

RS-Specialized-Instruct is the instruct-tuning dataset specifically targeting professional knowledge and skills in the fields of RS imagery. It aims to provide the necessary practical and professional knowledge foundation for RSVLMs. Details on its construction and composition are in Appendix D.

RS-ClsQaGrd-Instruct is the instruct-tuning dataset constructed from open-source RS scene classification, visual question answering, and visual grounding datasets, aiming to enhance the performance of RSVLMs on the above three tasks. We utilized predefined templates to transform the original datasets into instruct-tuning datasets suitable for VLMs. To eliminate uncertainty between tasks, we have assigned unique task identifiers for each task. Details are in Appendix E.

During the SFT process, we freeze the vision encoder, and finetune the LLM and the projection layer. We train for 1 epoch, using a batch size of 128, amounting to 1400 iterations. The same learning rate strategy is applied to finetune modules: a cosine schedule, with a base learning rate of $2e-5$. All SFT experiments were conducted on 8 NVIDIA A100-80G GPUs.

5 Experiment

We evaluated the performance of H²RSVLM on common RS visual tasks. More RS specific tasks are detailed in Appendix G. For information on the RS datasets used in the evaluation, please refer to Appendix F.

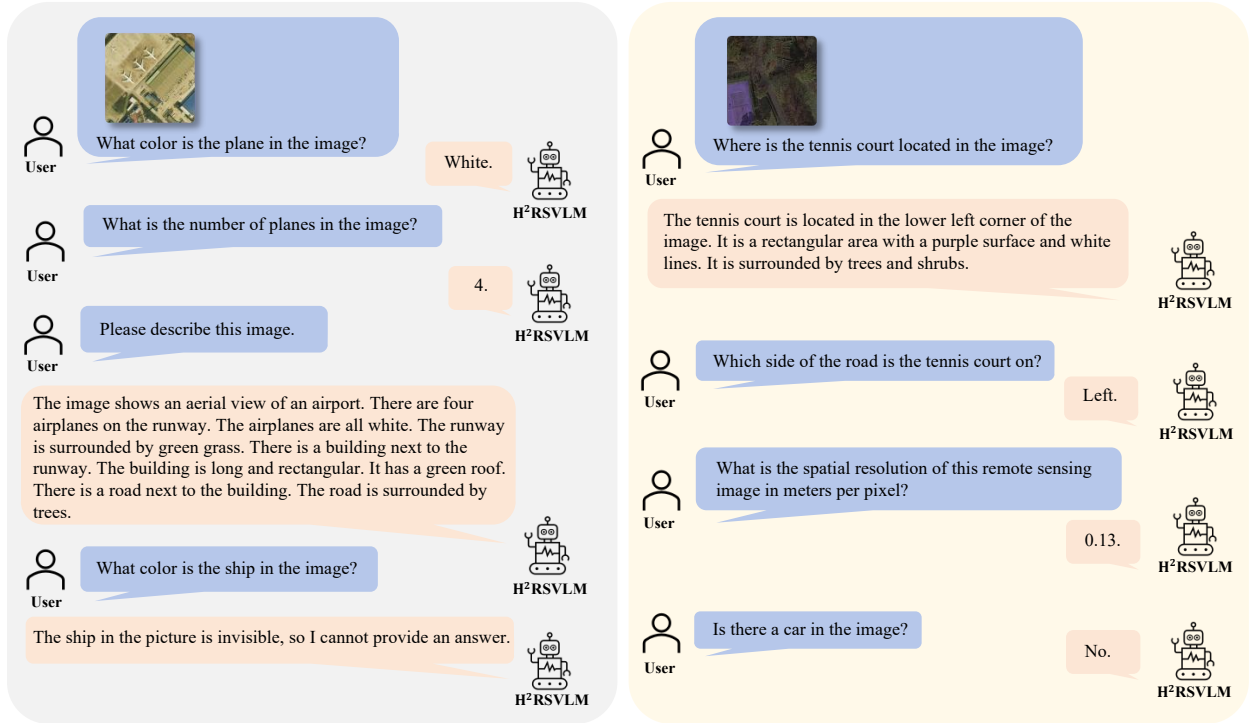


Fig. 6: Conversations between user and H²RSVLM.

5.1 Quantitative Results of Helpfulness

Scene Classification We evaluated the performance of H²RSVLM and other VLMs on five scene classification datasets including NWPU [7], METER-ML [71], SIRI-WHU [73], AID [58], and WHU-RS19 [13], as shown in Tab. 4. Our H²RSVLM surpasses the best generic VLM by 31.35% in terms of average accuracy, a significant increase that can be attributed to the domain knowledge our model possesses, which generic VLMs lack. Compared to the concurrent RSVLM, we still maintain an advantage, scoring 3.91 percentage points higher than LHRS-Bot [34]. Furthermore, H²RSVLM performs best on four datasets that include supervised learning and zero-shot tasks, demonstrating its excellent generalization capability.

Visual Question Answering We evaluated the performance of our model on the RSVQA-LR and RSVQA-HR datasets in RS visual question answering tasks. As shown in Tab. 5, we compared our model with other VLMs based on supervised learning accuracy on RSVQA-LR. The results for RSGPT were obtained after training independently on the RSVQA dataset for 5 epochs. Despite the significantly smaller training data used by H²RSVLM compared to other models, it still achieved competitive performance.

We also compared the zero-shot accuracy of the VLMs on the RSVQA-HR test set, as shown in Tab. 6. H²RSVLM performed best on average metrics, demonstrating its strong generalization capability.

These results suggest that H²RSVLM shows strong capabilities in tasks involving visual understanding at the image level.

Table 4: Accuracy of VLMs on the scene classification datasets. The underline means results of supervised learning, and others are all zero-shot learning.

Method	NWPU	METER-ML	SIRI-WHU	AID	WHU-RS19	Avg.
LLaVA-1.5 [28]	34.96	21.73	17.71	31.10	54.55	32.01
MiniGPTv2 [5]	28.15	14.29	35.46	32.96	64.80	35.13
Qwen-VL-Chat [3]	42.73	38.77	54.58	55.30	72.25	52.73
LHRS-Bot [34]	<u>83.94</u>	<u>69.81</u>	62.66	91.26	93.17	80.17
H ² RSVLM	93.87	71.68	68.50	89.33	97.00	84.08

Table 5: Accuracy of VLMs on visual question answering dataset RSVQA-LR. The results are all from supervised learning. Please note that the results for RSGPT were obtained after training on the entire RSVQA training dataset for 5 epochs.

Method	LR-rural	LR-presence	LR-compare	Avg.
RSGPT [19]	94.00	91.17	92.29	92.49
GeoChat [23]	91.09	90.33	94.00	91.81
SkyEyeGPT [65]	88.93	88.63	75.00	84.19
LHRS-Bot [34]	89.07	88.51	90.00	89.19
H ² RSVLM	88.00	89.58	89.79	89.12

Table 6: Accuracy of VLMs on visual question answering dataset RSVQA-HR. The results are all from **zero-shot** learning.

Method	HR-presence	HR-compare	Avg.
LLaVA-1.5 [28]	69.83	67.29	68.56
MiniGPTv2 [5]	40.79	50.91	45.85
Qwen-VL [3]	66.44	60.41	63.43
Geochat [23]	58.45	83.19	70.82
EarthGPT [69]	62.77	79.53	71.15
H ² RSVLM	65.00	83.70	74.35

Visual Grounding We evaluated the performance of H²RSVLM and other VLMs on the RS visual grounding (VG) task using the DIOR-RSVG test set, which comprises 7500 grounding samples involving images with dimensions of 800×800 pixels. We utilized accuracy@0.5 [23] as the evaluation metric, which determines the ratio of predicted boxes with an Intersection over Union (IoU) exceeding 0.5 with the ground truth boxes to the total number of test data. As shown in Tab. 7, despite the larger input sizes of the generic models compared to H²RSVLM, H²RSVLM still achieved the best performance, outperforming the second best CogVLM-Grounding-Generalist [50] by 3.46 percentage points. This showcases the excellent ability of our model in image fine-grained understanding and localization.

5.2 Quantitative Results of Honesty

We evaluated the performance of H²RSVLM and other VLMs on the RSSA test set, comparing their performance on answerable and unanswerable questions. The color task is an open-ended question, evaluated using ChatGPT for assessment. Details of the evaluation prompts and accuracy metrics calculation can be found in Appendix C. As shown in Tab. 8, generic open-source VLMs perform poorly on the unanswerable test set, especially qwen-chat, which achieves only 8.33% accuracy on unans-invis questions of **Color** task, lacking self-awareness ability to decline to answer. This also underscores the necessity of studying honest models with self-awareness.

Of course, some generic VLMs have the ability to decline to answer specific questions, such as cogvlm-chat [50] performing well on questions asking for the color of objects in panchromatic images. However, H²RSVLM achieved the best performance in 7 out of the 8 question subsets. Especially in the subset of question types where refusal to answer is needed, H²RSVLM achieved a significant margin in metrics, demonstrating its strong self-awareness capabilities. This is attributed to the involvement of our RSSA data in SFT stage.

5.3 Qualitative Results

In Fig. 6, we visualized examples of conversations between H²RSVLM and human users. In the multi-turn conversations, H²RSVLM not only can answer users’ questions about the existence of objects, object counts, object spatial positions, detailed descriptions of images, but also has the ability to answer professional questions in the RS field (such as estimating image GSDs). Furthermore, when faced unanswerable questions, it will explicitly refuse to respond to avoid causing hallucination. This demonstrates its helpfulness and honesty in the field of RS. More visualized results are shown in Appendix G.

Table 7: Performance of VLMs on visual grounding dataset DIOR-RSVG [64]. CogVLM* indicates the use of the cogvlm-grounding-generalist version.

Method	Input Size	Accuracy@0.5
CogVLM* [50]	490×490	44.58
Qwen-VL-chat [3]	448×448	31.86
H ² RSVLM	336×336	48.04

Table 8: Performance of VLMs on RSSA test set.

Method	Presence	Color			AbsPos		RelPos	
		ans	unans-pan	unans-invis	ans	unans	ans	unans
LLaVA-1.5 [28]	70.40	66.96	42.00	23.33	61.61	12.00	34.71	31.67
CogVLM [50]	74.71	31.25	100.00	68.00	33.93	16.67	29.34	11.00
Qwen-VL [3]	72.99	47.62	39.00	8.33	54.29	29.52	31.79	28.91
H ² RSVLM	82.47	83.04	85.00	93.33	82.14	83.67	53.72	78.00

Table 9: Performance of VLMs using different pretrain datasets. CntExs refers to the exact match metric for counting task. CntMAE refers to the Mean Absolute Error (MAE) [66] metric for counting tasks. RS5M-1.5M is a subset randomly selected from the RS5M, consisting of 1.5 million samples specifically chosen to investigate the quality of their captions. RS5M-5M represents the entire collection of 5 million samples.

Pretrain Dataset	#image	VG↑	Presence↑	Color↑	AbsPos↑	RelPos↑	CntEx↑	CntMAE↓
wo-pretrain	-	28.23	77.59	71.19	68.33	56.46	22.50	7.433
RS5M-5M [70]	5M	37.64	81.32	79.23	75.98	63.32	23.33	7.342
RS5M-1.5M [70]	1.5M	36.21	81.61	78.41	74.53	61.63	20.83	7.017
SkyScript [52]	1.5M	34.55	85.06	79.81	80.16	59.11	25.00	6.633
HqDC-1.4M	1.4M	51.06	81.32	85.85	85.96	71.51	27.50	6.525

5.4 Ablation Study

To validate the effectiveness of our HqDC-1.4M dataset, we conducted comparative experiments on various pre-training strategies as shown in Tab. 9. Specifically, we tested two types of strategies: 1) Removing the pre-training phase during model training and directly fine-tuning LLaVA pretrain model, referred to as the “wo-pretrain” strategy in the Tab. 9; 2) During the pre-training phase, replacing the HqDC-1.4M dataset with other RS visual language datasets such as RS5M [70] and SkyScript [52]. Note that, for fair comparison, the SFT dataset in the comparative experiments removed HqDC-Instruct Dataset containing a large number of dialogues and reasoning instructions.

As shown in Tab. 9, we evaluated six task metrics, including VG task, counting task², and all tasks in the RSSA test set. The results show that the “wo-pretrain” strategy performed the worst across all tasks, emphasizing the importance of using large-scale RS image-text dataset for the pretraining stage of RSVLMs. This result illustrates that in the stage of aligning the visual encoder and LLM, training a large-scale remote sensing model using only natural image-text pairs is insufficient, highlighting the crucial importance of utilizing large-scale RS image-text pairs. And further underscores the necessity of creating our dataset.

When comparing across different RS image-text datasets, the model trained using HqDC-1.4M achieved the best results across all datasets and tasks, including VG, RSSA, and the counting task. Specifically, the model achieved advantages of 13.42%, 5.80%, and 9.88%, in the visual grounding task, **AbsPos**, **RelPos** tasks, respectively, highlighting its superior performance in image local understanding and object localization compared to models trained on other datasets. The model also achieved similar optimal results on two types of metrics in the counting task. This further validates that the improvements in detailed image descriptions in HqDC-1.4M can enhance the model’s ability in fine-grained image understanding. The approach of using HqDC-1.4M in the color task resulted in a 6.04% advantage, credited to the object color descriptions missing in the other RS visual language datasets.

Additionally, we randomly selected 1.5 million samples from the RS5M [70] dataset for evaluation, referred to as RS5M-1.5M in Tab. 9. We noted that although RS5M-5M has more than three times the number of

² The counting task belongs to the RS-Specialized-Instruct dataset. Refer Appendix D for details.

training samples compared to RS5M-1.5M, the increase in performance is not substantial. Obviously, for the pretraining phase, having more training data is not necessarily better; the quality of the captions is more crucial.

6 Conclusion

We created HqDC-1.4M, which is a large-scale dataset consisting of 1.4 million pairs of remote sensing image and high-quality detailed caption. Additionally, we established the first dataset aimed at enhancing the self-awareness capabilities of RSVLM, named RSSA. These two datasets have significantly improved the performance of RSVLM in RS image understanding and spatial perception, and enhanced its honesty. Based on these datasets, we further developed H²RSVLM, the remote sensing vision language model that possesses both helpfulness and honesty. Through comprehensive experimental validation, H²RSVLM has demonstrated outstanding performance in various remote sensing visual tasks and can recognize and reject unanswerable questions, effectively mitigating the incorrect generations. The datasets we created only contain RS optical images and do not cover other type data, which limits the scope of the model’s applications. In the future, we plan to expand the existing RS multimodal large language models to support more types of data, thereby solving a broader range of remote sensing data analysis problems.

References

1. Abdalzaher, M.S., Soliman, M.S., El-Hady, S.M.: Seismic intensity estimation for earthquake early warning using optimized machine learning model. *IEEE Transactions on Geoscience and Remote Sensing* (2023) [1](#)
2. Achiam, J., Adler, S., Agarwal, S., Ahmad, L., Akkaya, I., Aleman, F.L., Almeida, D., Altenschmidt, J., Altman, S., Anadkat, S., et al.: Gpt-4 technical report. *arXiv preprint arXiv:2303.08774* (2023) [1](#), [3](#), [4](#)
3. Bai, J., Bai, S., Yang, S., Wang, S., Tan, S., Wang, P., Lin, J., Zhou, C., Zhou, J.: Qwen-vl: A frontier large vision-language model with versatile abilities. *arXiv preprint arXiv:2308.12966* (2023) [1](#), [9](#), [10](#), [11](#)
4. Brown, T., Mann, B., Ryder, N., Subbiah, M., Kaplan, J.D., Dhariwal, P., Neelakantan, A., Shyam, P., Sastry, G., Askell, A., et al.: Language models are few-shot learners. *Advances in neural information processing systems* **33**, 1877–1901 (2020) [1](#)
5. Chen, J., Zhu, D., Shen, X., Li, X., Liu, Z., Zhang, P., Krishnamoorthi, R., Chandra, V., Xiong, Y., Elhoseiny, M.: Minigtpt-v2: large language model as a unified interface for vision-language multi-task learning. *arXiv preprint arXiv:2310.09478* (2023) [1](#), [9](#), [10](#)
6. Chen, L., Li, J., Dong, X., Zhang, P., He, C., Wang, J., Zhao, F., Lin, D.: Sharegpt4v: Improving large multi-modal models with better captions. *arXiv preprint arXiv:2311.12793* (2023) [5](#)
7. Cheng, G., Han, J., Lu, X.: Remote sensing image scene classification: Benchmark and state of the art. *Proceedings of the IEEE* **105**(10), 1865–1883 (2017) [9](#), [23](#)
8. Cheng, Q., Sun, T., Liu, X., Zhang, W., Yin, Z., Li, S., Li, L., Chen, K., Qiu, X.: Can ai assistants know what they don't know? *arXiv preprint arXiv:2401.13275* (2024) [5](#)
9. Cherti, M., Beaumont, R., Wightman, R., Wortsman, M., Ilharco, G., Gordon, C., Schuhmann, C., Schmidt, L., Jitsev, J.: Reproducible scaling laws for contrastive language-image learning. In: *Proceedings of the IEEE/CVF Conference on Computer Vision and Pattern Recognition*. pp. 2818–2829 (2023) [8](#)
10. Chiang, W.L., Li, Z., Lin, Z., Sheng, Y., Wu, Z., Zhang, H., Zheng, L., Zhuang, S., Zhuang, Y., Gonzalez, J.E., Stoica, I., Xing, E.P.: Vicuna: An open-source chatbot impressing gpt-4 with 90%* chatgpt quality (March 2023), <https://lmsys.org/blog/2023-03-30-vicuna/> [4](#), [8](#)
11. Christie, G., Fendley, N., Wilson, J., Mukherjee, R.: Functional map of the world. In: *Proceedings of the IEEE Conference on Computer Vision and Pattern Recognition*. pp. 6172–6180 (2018) [4](#), [5](#), [23](#)
12. CrowdAI: Crowdai mapping challenge. <https://www.crowdai.org/challenges/mapping-challenge> (2018), accessed on: 2021-02-26 [5](#), [22](#)
13. Dai, D., Yang, W.: Satellite image classification via two-layer sparse coding with biased image representation. *IEEE Geoscience and Remote Sensing Letters* **8**(1), 173–176 (2011) [9](#), [23](#)
14. Demir, I., Koperski, K., Lindenbaum, D., Pang, G., Huang, J., Basu, S., Hughes, F., Tuia, D., Raskar, R.: Deepglobe 2018: A challenge to parse the earth through satellite images. In: *The IEEE Conference on Computer Vision and Pattern Recognition (CVPR) Workshops (June 2018)* [22](#)
15. Deng, Y., Zhao, Y., Li, M., Ng, S.K., Chua, T.S.: Gotcha! don't trick me with unanswerable questions! self-aligning large language models for responding to unknown questions. *arXiv preprint arXiv:2402.15062* (2024) [5](#)
16. Ding, J., Xue, N., Xia, G.S., Bai, X., Yang, W., Yang, M., Belongie, S., Luo, J., Datcu, M., Pelillo, M., Zhang, L.: Object detection in aerial images: A large-scale benchmark and challenges. *IEEE Transactions on Pattern Analysis and Machine Intelligence* pp. 1–1 (2021). <https://doi.org/10.1109/TPAMI.2021.3117983> [6](#), [7](#), [16](#)
17. Dosovitskiy, A., Beyer, L., Kolesnikov, A., Weissenborn, D., Zhai, X., Unterthiner, T., Dehghani, M., Minderer, M., Heigold, G., Gelly, S., et al.: An image is worth 16x16 words: Transformers for image recognition at scale. *arXiv preprint arXiv:2010.11929* (2020) [1](#), [2](#)
18. Driess, D., Xia, F., Sajjadi, M.S., Lynch, C., Chowdhery, A., Ichter, B., Wahid, A., Tompson, J., Vuong, Q., Yu, T., et al.: Palm-e: An embodied multimodal language model. *arXiv preprint arXiv:2303.03378* (2023) [1](#)
19. Hu, Y., Yuan, J., Wen, C., Lu, X., Li, X.: Rsgpt: A remote sensing vision language model and benchmark. *arXiv preprint arXiv:2307.15266* (2023) [1](#), [3](#), [10](#)
20. Hussain, S., Mubeen, M., Nasim, W., Mumtaz, F., Abdo, H.G., Mostafazadeh, R., Fahad, S.: Assessment of future prediction of urban growth and climate change in district multan, pakistan using ca-markov method. *Urban Climate* **53**, 101766 (2024) [1](#)
21. ISPRS: International society for photogrammetry and remote sensing: 2d semantic labeling challenge. <https://www.isprs.org/education/benchmarks/UrbanSemLab/2d-sem-label-potsdam.aspx> (2016) [22](#)
22. Kazemi Garajeh, M., Salmani, B., Zare Naghadehi, S., Valipoori Goodarzi, H., Khasraei, A.: An integrated approach of remote sensing and geospatial analysis for modeling and predicting the impacts of climate change on food security. *Scientific Reports* **13**(1), 1057 (2023) [1](#)
23. Kuckreja, K., Danish, M.S., Naseer, M., Das, A., Khan, S., Khan, F.S.: Geochat: Grounded large vision-language model for remote sensing. *arXiv preprint arXiv:2311.15826* (2023) [1](#), [3](#), [4](#), [10](#), [19](#), [20](#)

24. Li, C., Wong, C., Zhang, S., Usuyama, N., Liu, H., Yang, J., Naumann, T., Poon, H., Gao, J.: Llava-med: Training a large language-and-vision assistant for biomedicine in one day. *Advances in Neural Information Processing Systems* **36** (2024) [1](#)
25. Li, J., Li, D., Savarese, S., Hoi, S.: Blip-2: Bootstrapping language-image pre-training with frozen image encoders and large language models. *arXiv preprint arXiv:2301.12597* (2023) [4](#)
26. Li, J., Cheng, X., Zhao, X., Nie, J.Y., Wen, J.R.: Halueval: A large-scale hallucination evaluation benchmark for large language models. In: *The 2023 Conference on Empirical Methods in Natural Language Processing* (2023) [2](#)
27. Li, Y., Du, Y., Zhou, K., Wang, J., Zhao, W.X., Wen, J.R.: Evaluating object hallucination in large vision-language models. *arXiv preprint arXiv:2305.10355* (2023) [2](#), [17](#)
28. Liu, H., Li, C., Li, Y., Lee, Y.J.: Improved baselines with visual instruction tuning. *arXiv preprint arXiv:2310.03744* (2023) [1](#), [9](#), [10](#), [11](#)
29. Liu, H., Li, C., Wu, Q., Lee, Y.J.: Visual instruction tuning. *Advances in neural information processing systems* **36** (2024) [1](#), [3](#), [4](#), [6](#), [7](#), [8](#), [16](#)
30. Liu, L., Li, H.: Lending orientation to neural networks for cross-view geo-localization. In: *Proceedings of the IEEE/CVF conference on computer vision and pattern recognition*. pp. 5624–5633 (2019) [5](#)
31. Lobry, S., Marcos, D., Murray, J., Tuia, D.: Rsvqa: Visual question answering for remote sensing data. *IEEE Transactions on Geoscience and Remote Sensing* **58**(12), 8555–8566 (2020) [23](#)
32. Long, Y., Xia, G.S., Li, S., Yang, W., Yang, M.Y., Zhu, X.X., Zhang, L., Li, D.: On creating benchmark dataset for aerial image interpretation: Reviews, guidances and million-aid (2021) [4](#), [5](#)
33. Ma, Y., Cao, Y., Sun, J., Pavone, M., Xiao, C.: Dolphins: Multimodal language model for driving. *arXiv preprint arXiv:2312.00438* (2023) [1](#)
34. Muhtar, D., Li, Z., Gu, F., Zhang, X., Xiao, P.: Lhrs-bot: Empowering remote sensing with vgi-enhanced large multimodal language model. *arXiv preprint arXiv:2402.02544* (2024) [1](#), [3](#), [4](#), [9](#), [10](#), [19](#), [20](#)
35. Mustaqim, S.: Utilizing remote sensing data and arcgis for advanced computational analysis in land surface temperature modeling and land use property characterization. *World Journal of Advanced Research and Reviews* **21**(1), 1496–1507 (2024) [1](#)
36. OpenAI: Gpt-4v(ision) system card. <https://openai.com/research/gpt-4v-system-card> [1](#), [3](#)
37. Paiss, R., Ephrat, A., Tov, O., Zada, S., Mosseri, I., Irani, M., Dekel, T.: Teaching clip to count to ten. *arXiv preprint arXiv:2302.12066* (2023) [1](#)
38. Pang, C., Wu, J., Ding, J., Song, C., Xia, G.S.: Detecting building changes with off-nadir aerial images. *Science China Information Sciences* **66**(4), 1–15 (2023) [22](#)
39. Qu, B., Li, X., Tao, D., Lu, X.: Deep semantic understanding of high resolution remote sensing image. In: *2016 International conference on computer, information and telecommunication systems (Cits)*. pp. 1–5. IEEE (2016) [23](#)
40. Radford, A., Kim, J.W., Hallacy, C., Ramesh, A., Goh, G., Agarwal, S., Sastry, G., Askell, A., Mishkin, P., Clark, J., et al.: Learning transferable visual models from natural language supervision. In: *International conference on machine learning*. pp. 8748–8763. PMLR (2021) [1](#), [2](#), [3](#), [4](#)
41. Sorower, M.S.: A literature survey on algorithms for multi-label learning. *Oregon State University, Corvallis* **18**(1), 25 (2010) [22](#)
42. Sumbul, G., Charfuelan, M., Demir, B., Markl, V.: Bigearthnet: A large-scale benchmark archive for remote sensing image understanding. In: *IGARSS 2019-2019 IEEE International Geoscience and Remote Sensing Symposium*. pp. 5901–5904. IEEE (2019) [4](#)
43. Sun, X., Wang, P., Yan, Z., Xu, F., Wang, R., Diao, W., Chen, J., Li, J., Feng, Y., Xu, T., Weinmann, M., Hinz, S., Wang, C., Fu, K.: Fair1m: A benchmark dataset for fine-grained object recognition in high-resolution remote sensing imagery (2021) [6](#), [7](#), [16](#)
44. Team, G., Anil, R., Borgeaud, S., Wu, Y., Alayrac, J.B., Yu, J., Soricut, R., Schalkwyk, J., Dai, A.M., Hauth, A., et al.: Gemini: a family of highly capable multimodal models. *arXiv preprint arXiv:2312.11805* (2023) [2](#)
45. Tong, S., Liu, Z., Zhai, Y., Ma, Y., LeCun, Y., Xie, S.: Eyes wide shut? exploring the visual shortcomings of multimodal llms. *arXiv preprint arXiv:2401.06209* (2024) [1](#)
46. Tong, X.Y., Xia, G.S., Lu, Q., Shen, H., Li, S., You, S., Zhang, L.: Land-cover classification with high-resolution remote sensing images using transferable deep models. *Remote Sensing of Environment* **237**, 111322 (2020) [22](#)
47. Tong, X.Y., Xia, G.S., Zhu, X.X.: Enabling country-scale land cover mapping with meter-resolution satellite imagery. *ISPRS Journal of Photogrammetry and Remote Sensing* **196**, 178–196 (2023) [22](#)
48. Touvron, H., Martin, L., Stone, K., Albert, P., Almahairi, A., Babaei, Y., Bashlykov, N., Batra, S., Bhargava, P., Bhosale, S., et al.: Llama 2: Open foundation and fine-tuned chat models. *arXiv preprint arXiv:2307.09288* (2023) [1](#), [3](#), [8](#)
49. Wang, J., Zheng, Z., Ma, A., Lu, X., Zhong, Y.: Loveda: A remote sensing land-cover dataset for domain adaptive semantic segmentation. *arXiv preprint arXiv:2110.08733* (2021) [5](#)
50. Wang, W., Lv, Q., Yu, W., Hong, W., Qi, J., Wang, Y., Ji, J., Yang, Z., Zhao, L., Song, X., et al.: Cogvlm: Visual expert for pretrained language models. *arXiv preprint arXiv:2311.03079* (2023) [1](#), [10](#), [11](#)

51. Wang, Y., Liao, Y., Liu, H., Liu, H., Wang, Y., Wang, Y.: Mm-sap: A comprehensive benchmark for assessing self-awareness of multimodal large language models in perception. arXiv preprint arXiv:2401.07529 (2024) [2](#), [5](#)
52. Wang, Z., Prabha, R., Huang, T., Wu, J., Rajagopal, R.: Skyscript: A large and semantically diverse vision-language dataset for remote sensing. arXiv preprint arXiv:2312.12856 (2023) [2](#), [3](#), [4](#), [11](#)
53. Workman, S., Souvenir, R., Jacobs, N.: Wide-area image geolocalization with aerial reference imagery. In: Proceedings of the IEEE International Conference on Computer Vision. pp. 3961–3969 (2015) [5](#)
54. Wu, B., Zhang, M., Zeng, H., Tian, F., Potgieter, A.B., Qin, X., Yan, N., Chang, S., Zhao, Y., Dong, Q., et al.: Challenges and opportunities in remote sensing-based crop monitoring: a review. National Science Review **10**(4), nwac290 (2023) [1](#)
55. Wu, C., Zhang, L., Zhang, L.: A scene change detection framework for multi-temporal very high resolution remote sensing images. Signal Processing **124**, 184–197 (2016) [22](#)
56. Wu, T.H., Biamby, G., Chan, D., Dunlap, L., Gupta, R., Wang, X., Gonzalez, J.E., Darrell, T.: See, say, and segment: Teaching llms to overcome false premises. arXiv preprint arXiv:2312.08366 (2023) [2](#), [5](#)
57. Xia, G.S., Bai, X., Ding, J., Zhu, Z., Belongie, S., Luo, J., Datcu, M., Pelillo, M., Zhang, L.: Dota: A large-scale dataset for object detection in aerial images (2019) [6](#)
58. Xia, G.S., Hu, J., Hu, F., Shi, B., Bai, X., Zhong, Y., Zhang, L., Lu, X.: Aid: A benchmark data set for performance evaluation of aerial scene classification. IEEE Transactions on Geoscience and Remote Sensing **55**(7), 3965–3981 (2017) [9](#), [23](#)
59. Xia, R., Chen, J., Huang, Z., Wan, H., Wu, B., Sun, L., Yao, B., Xiang, H., Xing, M.: Crtranssar: A visual transformer based on contextual joint representation learning for sar ship detection. Remote Sensing **14**(6), 1488 (2022) [22](#)
60. Yin, Z., Sun, Q., Guo, Q., Wu, J., Qiu, X., Huang, X.: Do large language models know what they don't know? arXiv preprint arXiv:2305.18153 (2023) [5](#)
61. Yu, H., Zahidi, I.: Environmental hazards posed by mine dust, and monitoring method of mine dust pollution using remote sensing technologies: An overview. Science of The Total Environment **864**, 161135 (2023) [1](#)
62. Yuan, Z., Xiong, Z., Mou, L., Zhu, X.X.: Chatearthnet: A global-scale, high-quality image-text dataset for remote sensing. arXiv preprint arXiv:2402.11325 (2024) [3](#), [4](#)
63. Yuan, Z., Zhang, W., Fu, K., Li, X., Deng, C., Wang, H., Sun, X.: Exploring a fine-grained multiscale method for cross-modal remote sensing image retrieval. arXiv preprint arXiv:2204.09868 (2022) [23](#)
64. Zhan, Y., Xiong, Z., Yuan, Y.: Rsvg: Exploring data and models for visual grounding on remote sensing data. IEEE Transactions on Geoscience and Remote Sensing **61**, 1–13 (2023) [11](#), [17](#), [23](#)
65. Zhan, Y., Xiong, Z., Yuan, Y.: Skyeeygpt: Unifying remote sensing vision-language tasks via instruction tuning with large language model. arXiv preprint arXiv:2401.09712 (2024) [3](#), [10](#), [19](#), [20](#)
66. Zhang, C., Wang, S.: Good at captioning, bad at counting: Benchmarking gpt-4v on earth observation data. arXiv preprint arXiv:2401.17600 (2024) [11](#), [22](#)
67. Zhang, H., Diao, S., Lin, Y., Fung, Y.R., Lian, Q., Wang, X., Chen, Y., Ji, H., Zhang, T.: R-tuning: Teaching large language models to refuse unknown questions. arXiv preprint arXiv:2311.09677 (2023) [5](#)
68. Zhang, H., Liu, Y., Li, X., Feng, R., Gong, Y., Jiang, Y., Guan, X., Li, S.: Combing remote sensing information entropy and machine learning for ecological environment assessment of hefei-nanjing-hangzhou region, china. Journal of environmental management **325**, 116533 (2023) [1](#)
69. Zhang, W., Cai, M., Zhang, T., Zhuang, Y., Mao, X.: Earthgpt: A universal multi-modal large language model for multi-sensor image comprehension in remote sensing domain. arXiv preprint arXiv:2401.16822 (2024) [1](#), [3](#), [4](#), [10](#), [20](#)
70. Zhang, Z., Zhao, T., Guo, Y., Yin, J.: Rs5m: A large scale vision-language dataset for remote sensing vision-language foundation model. arXiv preprint arXiv:2306.11300 (2023) [2](#), [3](#), [4](#), [11](#)
71. Zhu, B., Lui, N., Irvin, J., Le, J., Tadwalkar, S., Wang, C., Ouyang, Z., Liu, F.Y., Ng, A.Y., Jackson, R.B.: Meter-ml: A multi-sensor earth observation benchmark for automated methane source mapping. arXiv preprint arXiv:2207.11166 (2022) [9](#), [23](#)
72. Zhu, D., Chen, J., Shen, X., Li, X., Elhoseiny, M.: Minigpt-4: Enhancing vision-language understanding with advanced large language models. arXiv preprint arXiv:2304.10592 (2023) [1](#)
73. Zhu, Q., Zhong, Y., Zhao, B., Xia, G.S., Zhang, L.: Bag-of-visual-words scene classifier with local and global features for high spatial resolution remote sensing imagery. IEEE Geoscience and Remote Sensing Letters **13**(6), 747–751 (2016) [9](#), [23](#)
74. Zorzi, S., Bittner, K., Fraundorfer, F.: Machine-learned regularization and polygonization of building segmentation masks. In: 2020 25th International Conference on Pattern Recognition (ICPR). pp. 3098–3105. IEEE (2021) [22](#)

A HqDC-1.4M Dataset

To ensure that Gemini-Vision model generates high-quality descriptions corresponding to remote sensing images, we carefully designed prompts as shown in Fig. 3. After obtaining the HqDC-1.4M dataset, we selected 140 pairs of image descriptions for accuracy evaluation in proportion to the number of images from the source dataset. Initially, we broke down each detailed description into sentences, totaling 851 sentences. Subsequently, two remote sensing experts jointly completed the manual evaluation task, categorizing the description sentences into three types: entirely accurate, partially accurate, and entirely incorrect. Through manual selection, the proportions of these three types were 68.9%, 20.2%, and 10.9%, confirming the quality assurance of the descriptions generated using Gemini-Vision. Tab. 10 provides detailed explanations of the sample detection quantities and type divisions. Fig. 7 displays multiple quality assessment examples.

Table 10: The sampled manual inspection results of HqDC-1.4M dataset.

Types	#Sentences	Proportion	Explanation
Entirely accurate	586	68.9%	Accurate and factual information that can be directly obtained from the image, without speculation.
Partially accurate	172	20.2%	The description has the following issues: inaccuracies in the relative position, color, motion status, shape, and orientation of the object; inclusion of information such as accurate resolution, building height, tree height, etc., which cannot be directly obtained from the image; inaccurate or incomplete object descriptions; speculation rather than statements regarding information such as geographical location, material, type, purpose, climate, etc.; and the use of inappropriate terms.
Entirely incorrect	93	10.9%	The entire sentence description is fabricated, incorrect judgments of high/low resolution, incorrect identification of image types, errors in quantity, and incorrect orientation.

B HqDC-Instruct Dataset

We followed the same approach as creating HqDC-1.4M to generate approximately 30k high-quality captions on the training sets of the DOTA-v2 [16], FAIR1M [43] datasets. We then used LLAVA’s method [29] to generate 26k multi-turn conversations and 4k complex reasoning instruction fine-tuning data tailored for remote sensing images. We will release all instruct data to advance the development of RSVLMs.

We used the language-only Gemini to create fine-tuning instruction data. The input prompts for Gemini include remote sensing image caption, object bounding boxes in the image, and provide two in-context examples. Detailed prompts and in-context examples of conversation and reasoning are shown in Tabs. 11 to 14.

As shown in Figure 8, we present an example from HqDC-Instruct dataset. The generated instructions are not only designed for conventional question-answering about objects in the image but also extend to complex reasoning.

C RSSA Dataset

In actual application scenarios, there are various types of unanswerable question types, and this paper, as an exploration in scientific research, is difficult to cover all types. Considering the changing factors such as lighting conditions and resolution in remote sensing images, overall, the visibility of objects in remote sensing images is lower compared to natural images. Therefore, in this paper, we have selected four tasks with the core of object presence in remote sensing images as the research scenario to explore the model’s

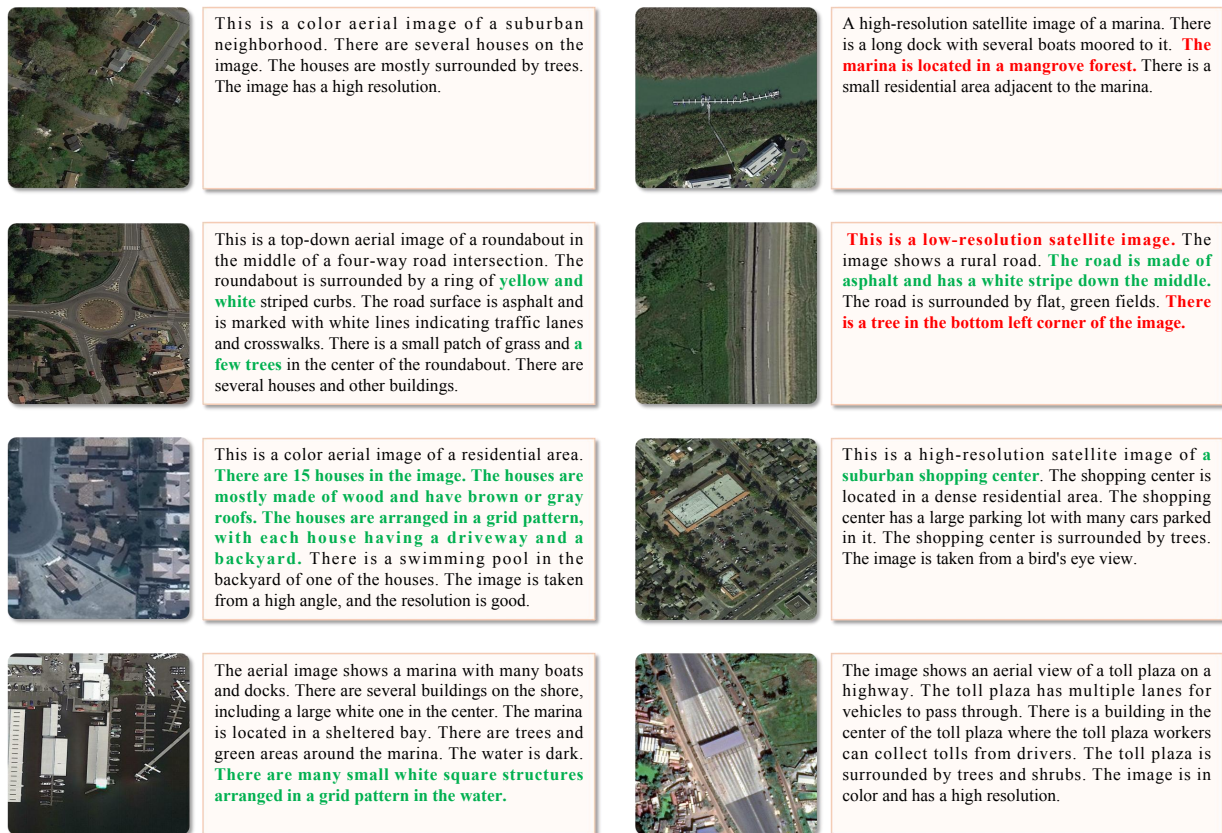


Fig. 7: Examples of HqDC-1.4M. **Black sentences** represent descriptions that are entirely accurate, **green sentences** represent descriptions that are partially accurate, and **red sentences** represent descriptions that are entirely incorrect.

self-aware capabilities. Based on the DOTA-v2 and Fair1M datasets, we have constructed the *Presence*, *Color*, *AbsPos*, and *RelPos* tasks. The following subsections will provide detailed explanations of our construction process and evaluation metrics.

C.1 Construction of *Presence* Task

If a certain type of object is included in the annotations of the original object detection dataset, then we can construct presence questions with the answer “Yes” based on this information. For questions with the answer “No”, we have adopted the method from [27] and constructed three types of samples: Random, Popular, and Adversarial. “Random” refers to randomly selecting a object from the categories in the original object detection dataset that is not present in the current image; “Popular” involves randomly selecting a object from the most numerous categories in the dataset that is not present in the current image; and “Adversarial” means first sorting these objects based on their co-occurrence frequency with the actual objects in the image, and then selecting the most common objects that have not appeared in the image. We use DOTA-v2-train and FAIR1M-train as the training set and DOTA-v2-test as the test set.

C.2 Construction of *Color* Task

When constructing dataset samples, we first extracted the color information of objects from the DOTA-v2 and FAIR1M datasets. We tried two methods to extract colors: the first method is to extract the RGB values of the pixels within the object contour and determine the object color based on established rules [64]; the second method is to use the “gemini-pro-vision” API to directly inquire about the object color. Specifically,

Table 11: System prompt for language-only Gemini model to conversation samples in HqDC-Instruct dataset.**System Prompt:**

You are an AI visual assistant, and you are seeing a single remote sensing or aerial image. What you see are provided with one detail sentences, describing the same image you are looking at. In addition, specific moving object locations within the image are given, along with detailed coordinates. These coordinates are in the form of bounding boxes, represented as [x1, y1, x2, y2, x3, y3, x4, y4] with floating numbers ranging from 0 to 1. Answer all questions as you are seeing the image. Design a conversation between you and a person asking about this image. The answers should be in a tone that a visual AI assistant is seeing the image and answering the question. Ask diverse questions and give corresponding answers. Include questions asking about the visual content of the image, including the object types, counting the objects, object actions, object appearance, relative positions between objects, etc.

Only include questions that have definite answers:

- (1) one can see the content in the image that the question asks about and can answer confidently;
- (2) one can determine confidently from the image that it is not in the image.

Do not ask any question that cannot be answered confidently. Also include complex questions that are relevant to the content in the image, for example, asking about background knowledge and function of the objects in the image, asking to infer the filming season in the image, etc. Again, do not ask about uncertain details. Provide detailed answers when answering complex questions. For example, give detailed examples or reasoning steps to make the content more convincing and well-organized. You can include multiple paragraphs if necessary. When using the information from the caption and coordinates, directly explain the scene, and do not mention that the information source is the caption or the bounding box. The generated dialogue should not include specific coordinates.

we slightly enlarged the rectangular box annotated for object detection, cropped out small images of that area, and then sent these small images to the Gemini-Vision model to ask about the color. We designed two different prompts and used the Gemini model to inquire about each cropped small image twice, and only confirmed the object color as accurately extracted when the results of both inquiries were consistent. The specific prompts can be seen in Tab. 15.

Through sampling checks, we found that the results of the second method were more accurate, so we adopted this method to extract the colors of objects in bulk from the DOTA-v2-train and FAIR1M-train datasets. For those objects whose colors were successfully extracted, we chose images that contained only a single object instance from the image and constructed answerable color questions (**ans**) based on a specific template, with the answer being the extracted color. As for the unanswerable questions, they fall into two categories: one is because the remote sensing image itself is panchromatic, so the color cannot be determined (**unans-pan**); the other is that the object inquired about in the question does not exist in the image (**unans-invis**). For the former, we use the panchromatic images from the DOTA-v2 dataset. For the latter, we constructed questions by referring to the “No” answer samples in the *Presence* task.

C.3 Construction of *AbsPos* and *RelPos* Task

In the *AbsPos* task, we divide the image evenly into nine regions and determine the object’s position within these regions according to specific rules, such as “left side,” “top right corner,” or “center,” etc. We specifically selected images that contain only one instance of object and built answerable question samples based on this. For the unanswerable question samples, we adopted the construction method used for the *Presence* task where the answer is “No.”

In the *RelPos* task, we listed all possible combinations of object types and filtered out images that contain only one instance of each type within the pair of combinations. We determined the relative position of these two objects based on the annotation information from the original object detection dataset, and constructed answerable question samples accordingly. For the unanswerable samples, we followed the approach used in the *Presence* task where the answer is “No,” selecting one or two objects that do not exist in the image to create the corresponding questions.

C.4 Metrics

We use a precise matching strategy to calculate the accuracy of three types: *Presence*, *AbsPos*, and *RelPos*. For the **ans** subset in the *Color* task, we also employ a exact matching strategy. However, for the **unans-pan** and **unans-invis** tasks, we utilize the ChatGPT-3.5 API for evaluation, with specific prompts

Table 12: In-context examples for language-only Gemini model to conversation samples in HqDC-Instruct dataset.**In-context examples:****User:**

“The caption of the image is as follows: This is an aerial image of four tennis courts. The courts are made of green concrete with fake grass and have white lines. They are arranged in a square, with two courts on each side. There is a small space between each court, which is covered with red clay. There is a fence around the entire complex. There are trees and bushes outside the fence. The category and location of objects in image are as follows: tennis-court: [0.916,0.6172,0.998,0.623, 0.998,0.9668,0.8926,0.9609]. tennis-court: [0.5156,0.5957,0.6758,0.6055, 0.6562,0.9453,0.4961,0.9375]. tennis-court: [0.2598,0.5781,0.418,0.5879, 0.3965,0.9297,0.2383,0.9199]. tennis-court: [0.5508,0.002,0.7109,0.002, 0.6934,0.2891,0.5352,0.2812]. tennis-court: [0.2891,0.002,0.4512,0.002, 0.4355,0.2734,0.2734,0.2617].”

AI:

“**Q:** Can you count the number of tennis courts in the image? **A:** Certainly! I can see a total of five tennis courts in the image.

Q: What is the material used for the courts? **A:** The courts are made of green concrete with fake grass and have white lines.

Q: Is there any space between the courts? **A:** Yes, there is a small space between each court, which is covered with red clay.

Q: Is there any fence around the courts? **A:** Yes, there is a fence around the entire complex.

Q: Can the tennis court seen in the image be used to host large-scale matches or events? **A:** The image shows that there are no spectator stands around the tennis court, which may indicate that it’s less likely to be used for hosting large-scale matches or events. Generally, such matches or events require spectator stands to accommodate audiences. However, this does not mean that the tennis court cannot host any matches or events. It could be used for smaller-scale activities, such as community matches, school matches, or training sessions. Additionally, if there’s sufficient space, temporary stands could potentially be set up. Overall, the lack of spectator stands might suggest that this tennis court is more likely used for leisure or training, rather than hosting large-scale matches or events.”

User:

“The caption of the image is as follows: This is a high-resolution satellite image of an airport. There are two airplanes on the tarmac. The airplanes are both white and blue. The one on the left is a little bigger than the one on the right. There are also a few cars and trucks on the tarmac. The cars and trucks are all black or gray. The tarmac is made of concrete and has a lot of cracks in it. There is a building next to the tarmac. The building is made of glass and metal. There are a few trees around the building. The trees are all green. The category and location of objects in image are as follows: plane: [0.6836,0.4805,0.998,0.4805, 0.998,0.998, 0.6836,0.998]. plane: [0.002,0.4609,0.4648,0.4609, 0.4648,0.998,0.002,0.998]. large-vehicle: [0.5,0.7305,0.5273,0.7305, 0.5352,0.8691,0.5059,0.8691]. small-vehicle: [0.625,0.7539,0.625,0.7773, 0.5801,0.7734,0.5859,0.752]. small-vehicle: [0.2988,0.4141,0.3125,0.4121, 0.3125,0.4492, 0.2969,0.4492]. small-vehicle: [0.3203,0.3379,0.3203,0.3145, 0.373,0.3145,0.3711,0.3379]. large-vehicle: [0.0508,0.3477,0.0488,0.3203, 0.1602,0.3184,0.1602,0.3438]. small-vehicle: [0.8789,0.002,0.8984,0.002, 0.8945,0.043,0.875,0.043]. small-vehicle: [0.9043,0.002,0.9258,0.002, 0.9199,0.0488,0.9004,0.0469]. small-vehicle: [0.998,0.2852,0.998,0.3145, 0.9453,0.3145,0.9434,0.2891].”

AI:

“**Q:** How many airplanes are there on the tarmac? **A:** There are two airplanes on the tarmac. **Q:** Can you describe the appearance of the airplanes? **A:** Both airplanes are white and blue in color. The one on the left is slightly bigger than the one on the right. **Q:** Are there any cars and trucks on the tarmac? **A:** Yes, there are cars and trucks on the tarmac. **Q:** What colors are the cars and trucks? **A:** The cars and trucks on the tarmac are all black or gray in color. **Q:** When was the largest moving object in the image invented? The largest moving object in the image is an airplane, which was invented in the early 20th century. The Wright brothers, Orville and Wilbur, conducted the first successful manned, powered flight on December 17, 1903. Their aircraft, known as the “Wright Flyer”, made its first flight in Kitty Hawk, North Carolina, USA. Although this flight lasted only 12 seconds, it marked the beginning of human flight.”

detailed in Tab. 16. The accuracy of all subsets is represented as the ratio of correctly answered questions to the total number of questions.

For the *Presence* task where unanswerable questions do not exist, only the **ans** subset needs to be calculated. For the *AbsPos* and *RelPos* tasks, both the **ans** and **unans** subsets need to be considered to calculate the average accuracy, denoted as Acc , where Acc_{ans} represents the accuracy of the **ans** subset, and Acc_{unans} represents the precision of the **unans** subset. The overall accuracy, Acc , can be calculated as:

$$Acc = (Acc_{ans} + Acc_{unans})/2.0.$$

For the *Color* task, the overall accuracy, Acc_{color} , can be calculated using the following formula:

$$Acc_{color} = (Acc_{ans} + (Acc_{unans-pan} + Acc_{unans-invis})/2.0)/2.0,$$


Where Acc_{ans} , $Acc_{unans-pan}$, and $Acc_{unans-invis}$ are the accuracies of the **ans** subset, **unans-pan** subset, and **unans-invis** subset, respectively.

D RS-Specialized-Instruct Dataset

Existing RSVLMs [23, 34, 65] mostly focus on generic tasks such as visual grounding (VG), image classification, which are also common tasks in natural images. However, for remote sensing images, their application

Table 13: System prompt for language-only Gemini model to complex reasoning samples in HqDC-Instruct dataset.

System Prompt:
 You are an AI visual assistant that can analyze a single remote sensing image. You are given a sentence that describes the same image you’re observing. In addition, specific moving object locations within the image are given, along with detailed coordinates. These coordinates are in the form of bounding boxes, represented as $[x1, y1, x2, y2, x3, y3, x4, y4]$ with floating numbers ranging from 0 to 1. The task is to use the provided caption and rotate bounding box information, create a plausible question about the image, and provide the answer in detail. Create complex questions beyond describing the scene. To answer such questions, one should require first understanding the visual content, then based on the background knowledge or reasoning, either explain why the things are happening that way, or provide guides and help to user’s request. Make the question challenging by not including the visual content details in the question so that the user needs to reason about that first. Instead of directly mentioning the bounding box coordinates, utilize this data to explain the scene using natural language. Include details like object counts, position of the objects, relative position between the objects. When using the information from the caption and coordinates, directly explain the scene, and do not mention that the information source is the caption or the rotate bounding box. Always answer as if you are directly looking at the image.



Conversation

Q: How many docks are there with boats moored to them?
A: I can see that there are several docks with boats moored to them, but the exact number is difficult to determine from this image.

Q: What is the color of the water in the marina?
A: The water in the marina has a dark blue color.

Q: Are there any boats in the marina that are particularly large or different from the others?
A: The image doesn't show any boats that are significantly larger or visually distinct from the others.

Q: How many harbors are seen in the image?
A: There appear to be four harbors in the image.

Q: What type of boats are docked in the marina?
A: Unfortunately, the resolution of the image doesn't allow me to distinguish the specific types of boats docked in the marina.

Reasoning

Q: If a boat race is to be organized in the marina, which of the four harbors would be the most suitable starting point for the race, considering factors like wind direction, water currents, and proximity to obstacles?
A: To determine the most suitable starting point for the boat race, several factors need to be taken into account. Firstly, the wind direction can play a crucial role in the race. If the wind is blowing consistently from a particular direction, it can provide an advantage to boats starting in that direction. Secondly, the water currents can also affect the speed and direction of the boats. Starting in a harbor that is less affected by strong currents can give boats a better chance of maintaining their course. Lastly, the proximity of obstacles such as docks, buoys, and other boats should be considered to ensure a safe start for the race. By carefully evaluating these factors, the most suitable starting point can be chosen to ensure a fair and exciting race.

Fig. 8: Examples of HqDC-Instruct Dataset.

scenarios are not limited to the tasks mentioned above. We believe that RSVLMs should have more remote sensing-specific functionalities. As shown in Tab. 17, we explored five categories of remote sensing-specific tasks including image ground sampling distance estimation (GSDEst), image type identification (ImgType), object measurement (ObjMeas), multi-label landcover classification (MLC), and building footprint vectorization (BFV). In addition, we also included counting ability, which was not evaluated in previous work, making a total of six tasks. The table also provides detailed information about this dataset.

E RS-ClsQaGrd-Instruct Dataset

Following previous RSVLMs research [23, 34, 65, 69], we constructed a multi-task instruct dataset using public remote sensing datasets, covering tasks such as scene classification, visual question answering, and visual grounding, named as the RS-ClsQaGrd-Instruct dataset. The composition of this dataset is shown in Tab. 18. Specific token identifiers were set for each task when constructing this dataset, as detailed in Tab. 18. Please note that in this paper, the x and y coordinates involved in tasks such as VG have a value range from 000 to 999, which is normalized based on the corresponding image size.

Table 14: In-context examples for language-only Gemini model to complex reasoning samples in HqDC-Instruct dataset.**In-context examples:****User:**

“The caption of the image is as follows: This is a black and white aerial image of an airport. There are two runways and several planes on the ground. The planes are parked at the gates near the terminal. There is a large shadow of the plane on the runway. The category and location of objects in image are as follows: plane: [0.1797,0.8711,0.2715,0.8574, 0.293,0.9512, 0.1934,0.9668]. plane: [0.5137,0.6641,0.4492,0.5859, 0.5312,0.5156, 0.5918,0.5938]. plane: [0.0254,0.2461,0.1152,0.2246, 0.1406,0.3262, 0.0469,0.3496].”

AI:

Q: What are the possible reasons for the presence of a large shadow of a plane on the runway? **A:** The large shadow of a plane on the runway can be attributed to a few factors. Firstly, the angle at which the sunlight hits the aircraft plays a significant role in the size and visibility of the shadow. The lower the angle of the sun, the longer and more prominent the shadow will be. This is often seen during the morning or evening when the sun is closer to the horizon. Additionally, the size of the aircraft itself can also affect the size of the shadow. Larger aircraft, such as wide-body jets, tend to cast longer shadows compared to smaller aircraft like private planes. Furthermore, the weather conditions can influence the visibility of the shadow. Clear skies and direct sunlight create the most favorable conditions for a prominent shadow, while cloudy or overcast conditions can make it less visible.”

User:

“The caption of the image is as follows: The image is a high-resolution panchromatic aerial image. It is a top-down view of a residential area. There are many houses in the image. The houses are mostly made of concrete and have a variety of shapes and sizes. The houses are arranged in a grid pattern. The roads in the image are made of asphalt and are lined with trees. There are also some trees in the yards of the houses. The image is taken in the summer. The category and location of objects in image are as follows: roundabout: [0.0547,0.4199,0.1074,0.4199, 0.1074,0.4707, 0.0547,0.4707].”

AI:

Q: If a new housing development is planned in the northern part of the neighborhood, how would the traffic flow be affected during the construction phase, and what measures could be taken to minimize the impact? **A:** The construction of a new housing development in the northern part of the neighborhood is likely to have an impact on the traffic flow in the area. During the construction phase, there will be an increase in heavy vehicles transporting materials and equipment to and from the site. This can lead to traffic congestion and delays, particularly on the roads leading to and from the development. To minimize the impact, traffic management measures such as temporary traffic signals, detours, and road closures may be implemented. Additionally, staggering the work hours of construction workers and scheduling deliveries and pickups outside of peak traffic times can help reduce congestion. Furthermore, providing clear signage and directions to the construction site can help drivers navigate the area more easily. By implementing these measures, the impact of construction traffic on the neighborhood’s traffic flow can be mitigated.”

User:

F Evaluated Test Datasets

In the main paper, we conducted quantitative evaluations on all task types in the RSSA and RS-ClsQaGrd-Instruct datasets. The test sets for the RSSA are reported in the main paper. For the evaluation of tasks in the RS-ClsQaGrd-Instruct dataset, we selected the test sets from publicly available datasets, as shown in Tab. 19.

G More Results of H²RSVLM

For the tasks on RS-Specialized-Instruct dataset, we conducted a quantitative evaluation of the performance of the H²RSVLM. As shown in the last column of Tab. 17, we chose appropriate evaluation metric for different tasks. Given that current VLMs and RSVLMs have not yet achieved the capability to handle such specialized remote sensing tasks, we did not compare the H²RSVLM with them. Nevertheless, to further the advancement of RSVLMs, we have still reported the evaluation metrics and the performance of H²RSVLM in detail.

To provide a more intuitive demonstration of the remote sensing specific tasks we studied and the performance of H²RSVLM, we have visualized some sample results in Figs. 9 to 15. From the perspective of quantitative assessment and visualization of results, aside from there being significant room for performance improvement in VG and BFV tasks, the H²RSVLM generally performs quite well in other tasks. In the BFV task, H²RSVLM can only perform well on relatively simple contours, and it struggles with complex contours. As for the VG task, as shown in Fig. 14, H²RSVLM excels at handling large objects but falls short in scenarios with small objects. This may be due to the limitations of H²RSVLM in terms of image input size (336 × 336 pixels).

Table 15: Prompts for Gemini-Vision model to extract the color of the object in the cropped image.**Prompt1:**

There is a {obj} in the center of the given image. Please tell me the color of this object. Just tell me the color.

Prompt2:

In the provided image, there is a {obj} at the center. Could you please specify the color of this object? Provide only the color.

Table 16: Prompts for gpt-3.5-turbo model to evaluate color tasks.**Prompt of unans-pan:**

You are an AI assistant, and you need to evaluate a description provided by the user. If the description contains the meaning "This image is in black and white, and the actual colors cannot be determined.", you should return 1; otherwise, return 0. Example 1: Input:The actual color of the storage tank cannot be determined from this remote sensing image as it is in grayscale. Remote sensing images are typically in black and white or grayscale due to the limitations of the sensors used, which capture light without color differentiation. Output:1 Example 2: Input:The storage tank in the remote sensing image is black. Your output:0 Example 3: Input:{pred} Output:

Prompt of unans-invis:

You are an AI assistant, and you need to assess a description provided by the user. If the description contains the meaning "The target is not visible in the image, or the target does not exist.", you should return 1; otherwise, return 0. Example 1:Input:The actual color of the airport in the remote sensing image is green. This is because the image is a satellite or aerial photograph, and green is typically used to represent vegetation or land cover. Output:0 Example 2:There is no existence of a ship in the image description.Your output:1 Example 3: Input:{pred} Output:

Table 17: Details of RS-Specialized-Instruct Dataset and Performance of H²RSVLM. OE means open-ended. MAE [66] means mean absolute error. C-IoU [74] means complexity aware IoU. F_1 [41] means example-based F_1 -Measure.

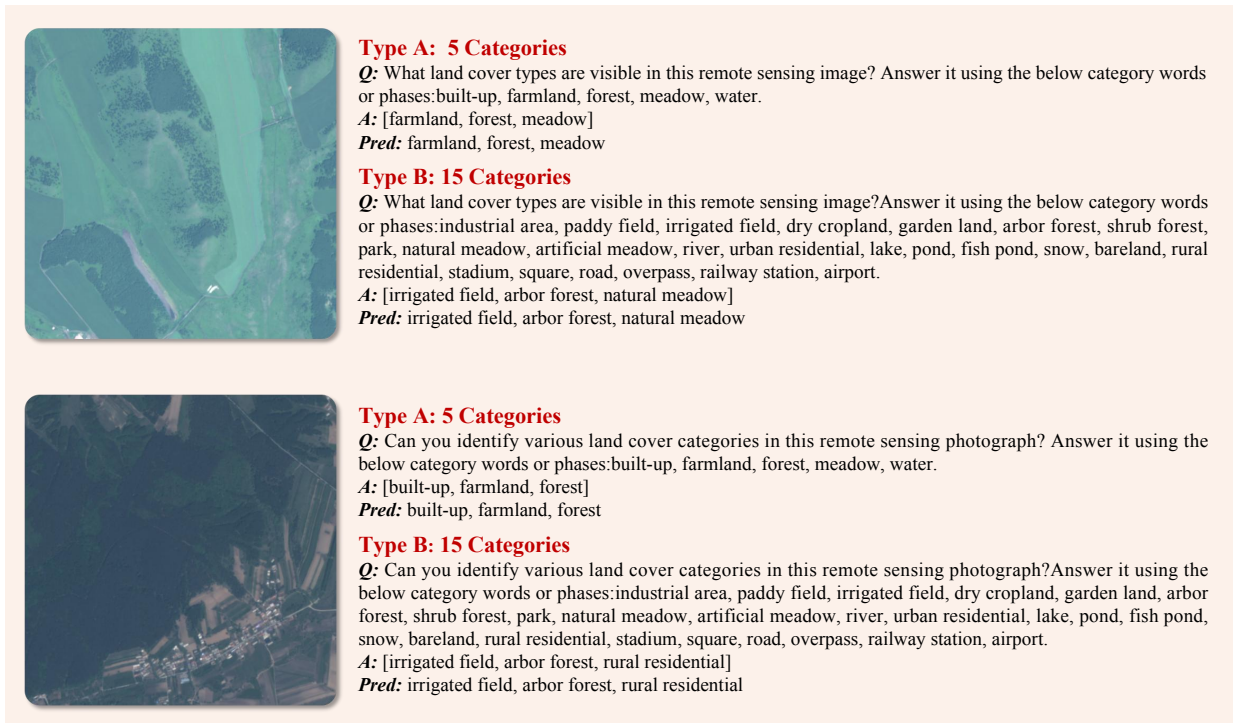
Task	Qn. Type	Train Img Src	Test Img Src	#Train Sample	#Test Sample	Test Perf.
ImgType	MCQ	BANDON-train [38] MtS-WH-train [55] DOTA-v2-train MSAR-train [59]	BANDON-test MtS-WH-test DOTA-v2-test Potsdam [21] MSAR-test	400	20	Acc: 95.00%
GSDEst	OE	DOTA-v2-train FAIR1M-train fMoW-train	DOTA-v2-test FBP [47]	3000	100	MAE: 0.217
ObjMeas	OE	DOTA-v2-train FAIR1M-train	DOTA-v2-test FAIR1M-val	3000	100	MAE: 14.08
BFV	OE	CrowdAI-train [12]	CrowdAI-val	10000	200	C-IoU: 70.41%
MILc	OE	GID-train [46] FBP-train DeepGlobe-train [14]	GID-test FBP-test	6000	6240 6240	F_1 : 85.77% F_1 : 72.20%
Counting	OE	CrowdAI-train DOTA-v2-train	DOTA-v2-test	7000	120	MAE: 6.22

Table 18: Detailed introduction of the RS-ClsQaGrd-Instruct datasets. The * indicates that the dataset has been duplicated twice, with the aim of enhancing the model’s learning efficiency on that task.

Dataset (Trainset)	Samples	Task Type	Specific Form of the Question
RSVQA-LR [31]	10000	VQA	{VQA}
fMoW [11]	4969	Classification	
METER-ML [71]	1497	Classification	{CLS} Classify the image within one of the given classes
NWPU [7]	4995	Classification	
RSITMD [63]	484	Classification	
UCM [39]	2100	Classification	
DIOR-RSVG [64]	27000*	Visual Grounding	{VG} Object expression

Table 19: Detailed introduction of the test datasets.

Dataset (Testset)	Task Type	Img size	Resolution (m)	Categories
AID [58]	Classification	600×600	0.5 – 8	30
METER-ML [71]	Classification	720×720	1	6
NWPU [7]	Classification	256×256	0.2 – 30	45
SIRI-WHU [73]	Classification	200×200	2	12
WHU-RS19 [13]	Classification	600×600	– 0.5	19
RSVQA-LR [31]	VQA	256×256	10	–
RSVQA-HR [31]	VQA	512×512	0.15	–
DIOR-RSVG [64]	Visual Grounding	800×800	0.5 – 30	20

**Fig. 9:** Examples of the results from multi-label landcover classification task.

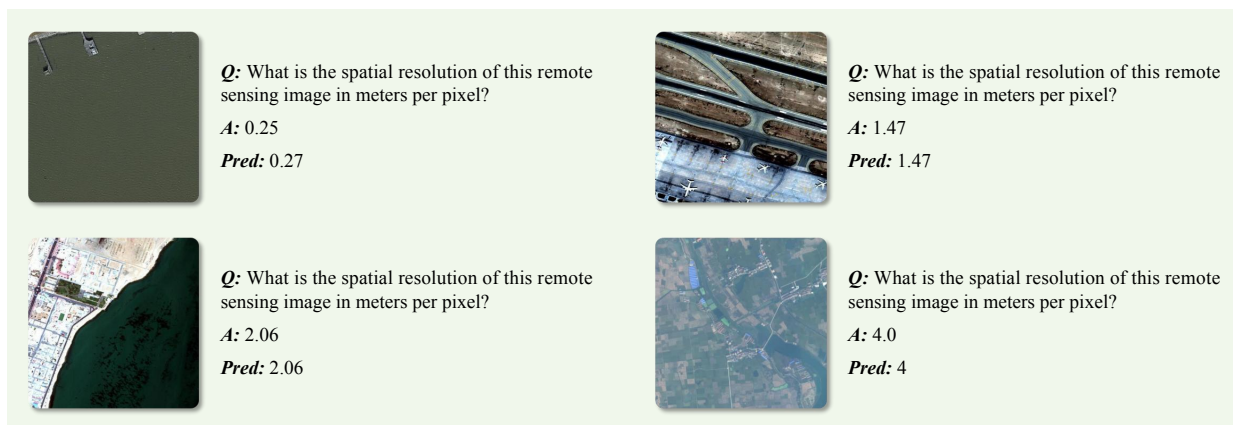


Fig. 10: Examples of the results from image ground sampling distance estimation task.

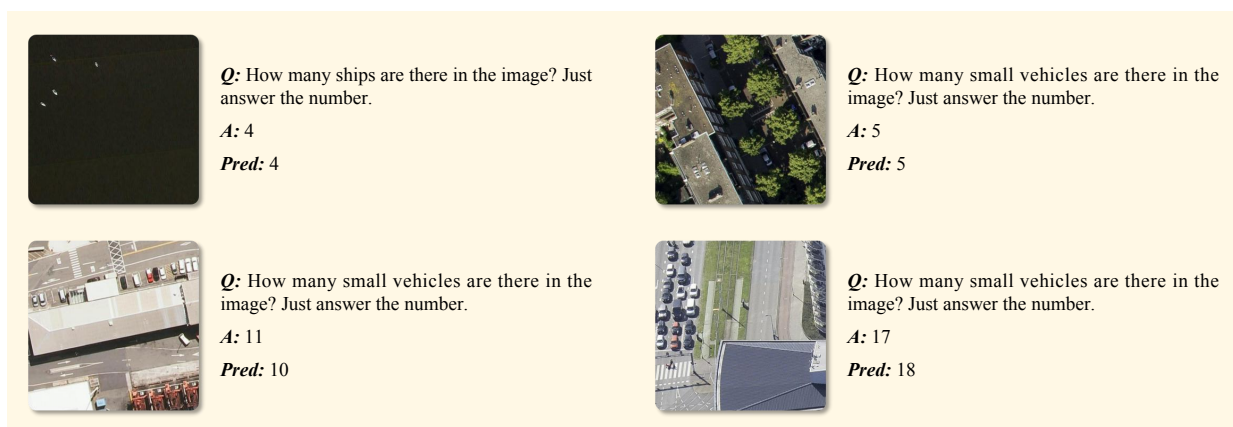


Fig. 11: Examples of the results from counting task.

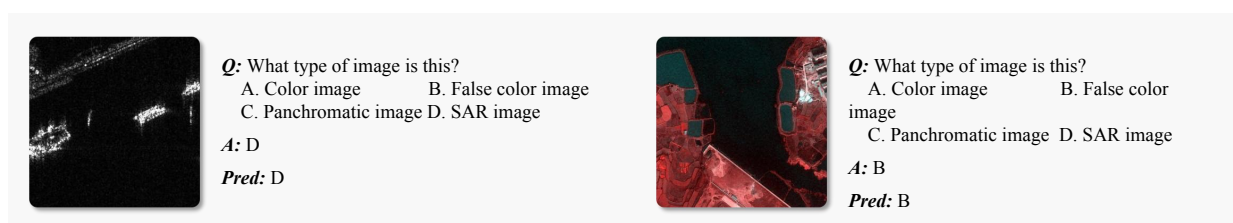


Fig. 12: Examples of the results from image type identification task.

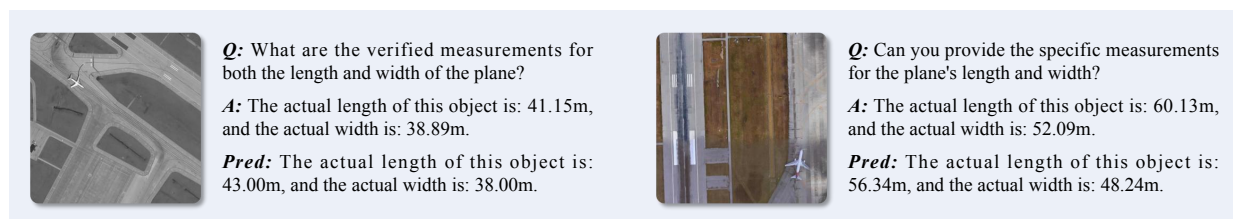


Fig. 13: Examples of the results from image type identification task.

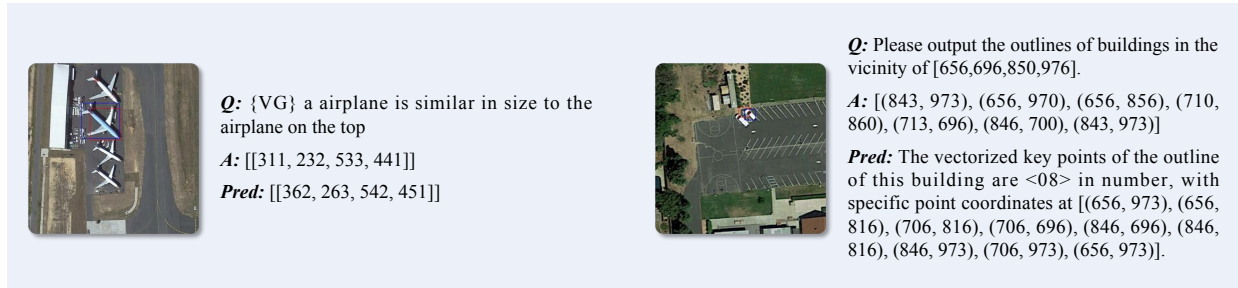


Fig. 14: Examples of the results from visual grounding task. The red box represents the predicted result, while the blue box represents the ground truth.

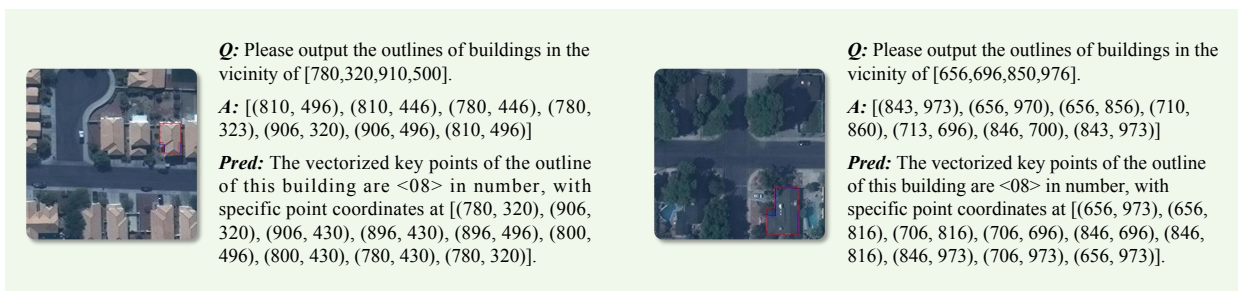


Fig. 15: Examples of the results from building footprint vectorization task. The red polygon represents the predicted result, while the blue polygon represents the ground truth.